Wind-structure interaction simulations of wind induced ovalling vibrations in silo groups

J. Hillewaere[1], J. Degroote[2], G. Lombaert[1], J. Vierendeels[2], and G. Degrande[1]

[1]Department of Civil Engineering, KU Leuven, Kasteelpark Arenberg 40, B-3001 Heverlee, Belgium, *jeroen.hillewaere@bwk.kuleuven.be*.
[2]Department of Flow, Heat and Combustion Mechanics, Ghent University, St. Pietersnieuwstraat 41, B-9000 Gent, Belgium.

Abstract

Wind induced ovalling vibrations have been reported to occur on several empty, flexible silo structures in group arrangement. The focus in this paper is on the numerical prediction of this phenomenon by simulating the wind flow around a single silo and taking into account the interaction of the wind flow with the structural response. The importance of the 3D turbulent wind flow and wake effects on the aerodynamic pressures on the silo is investigated using 3D CFD simulations. The wind-structure interaction phenomenon is subsequently studied using a one-way coupling and a two-way coupling approach. The present results show reasonable qualitative agreement with observations.

1 Introduction

Wind induced ovalling vibrations were observed during a storm in October 2002 on several empty silos of a closely spaced group consisting of 8 by 5 thin-walled silos in the port of Antwerp (Dooms *et al.*, 2006). To clarify the cause of these wind induced silo vibrations, computational fluid dynamics (CFD) simulations are an interesting alternative to more expensive wind tunnel tests or in situ measurements. In the present paper, the focus is therefore on the 3D CFD simulation of the wind flow around a single silo.

The wind-structure interaction phenomenon is first studied by applying the 3D aerodynamic pressures as transient external loads on a 3D finite element model of the silo. In this one-way coupling approach, no interaction effects are taken into account and only forced resonance due to turbulent wind fluctuations in the incoming or wake flow can be investigated. Afterwards, a two-way coupling simulation is considered where the coupled problem of wind flow and structure is solved, hence taking into account possible interaction effects due to the deforming fluid domain. Because the computational effort to perform such fully coupled wind-structure interaction simulation is much larger, it is interesting to assess the necessity of solving the coupled problem as a whole.

2 Wind flow simulations

For the present purpose, 3D CFD simulations are performed to determine the aerodynamic pressures acting on the silo surfaces exposed to the incoming turbulent wind. It is important that these pressures are predicted accurately. Therefore, the numerical treatment of turbulence in the wind flow has to be considered with care. The governing incompressible Navier-Stokes equations are discretized by means

of the finite volume method in the commercial software package Fluent 14.0 (2011). Because a high Reynolds number wind flow is considered, it is impossible to solve this nonlinear set of discretized equations exactly with all details. Instead, turbulence models have to be used. The applied technique is chosen mainly for accuracy but also in the light of achieving results within a reasonable computation time.

Two turbulence modelling approaches can be considered in general. The first are the RANS (Reynolds-averaged Navier-Stokes) procedures where Reynolds averaging is applied and turbulence is modelled. The second approach are large eddy simulations (LES) where a spatial filter is used to distinguish between large turbulent eddies that are resolved and eddies smaller than the filter size that are modelled. For highly turbulent flows, it is in practice impossible to use LES simulations because of the prohibitive grid requirements to model the small turbulent eddies in near-wall flows. RANS methods on the other hand are quite effective in the near wall regions but yield insufficient accuracy in separated regions, where large unsteady turbulence scales are dominant. For this reason hybrid RANS/LES methods have been proposed, such as detached eddy simulations (DES, Spalart *et al.*, 1997). In this work, a delayed DES approach (DDES) is applied in which a shielding function is used to ensure that RANS is used in the entire near-wall region (Menter & Kuntz, 2002). A snapshot of the turbulence intensity in a DDES simulation is shown in figure 1. This result shows a much more realistic modelling of turbulence in the wake of the cylinder when compared to typical RANS simulations where large-scale vortices are artificially preserved with very wide, unrealistic wake regions as a result.

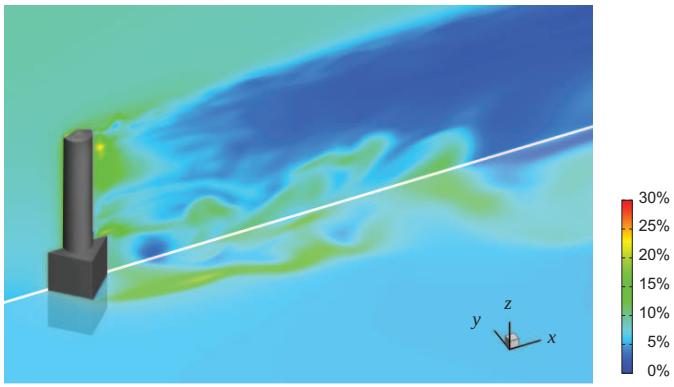

Figure 1: Turbulence intensity in the flow around a single silo structure, calculated with 3D DDES, for an angle of incidence $\alpha = 45^\circ$ at $t = 60.0\,\mathrm{s}$. The turbulence intensity is shown in a vertical plane and a horizontal plane at mid-height of the prismatic building below the silo.

Since the specific atmospheric conditions near the silo group in Antwerp were not monitored at the time that the ovalling vibrations were observed, approximate wind conditions have been set up, based on the location of the group and statistical wind data for storm conditions in design codes. For the atmospheric boundary layer (ABL), realistic power law velocity and turbulence profiles (Tominaga *et al.*, 2008) are imposed at the inlet of the computational domain while for the generation of fluctuating velocity components, a spectral synthesizer method is used as proposed by Kraichnan (1970) and modified by Smirnov *et al.* (2001).

3 Structural model and ovalling mode shapes

In order to determine the structural response to a dynamic wind load, a numerical finite element (FE) model of the silo structure is introduced. This model also allows to calculate the ovalling mode shapes and corresponding natural frequencies of the silo structure.

Ovalling deformations of a thin-walled shell structure are defined as a deformation of the cross section of the structure without bending deformation with respect to the longitudinal axis of symmetry (Païdoussis *et al.*, 1982). The ovalling mode shapes for the thin-walled empty silos (diameter D = 5.5 m and wall thickness t_s = 0.07 m – 0.10 m, varying along the height of the silo) are referred to by a couple (m, n) where m denotes the half wave number in the axial direction and n is the number of circumferential waves (figure 2).

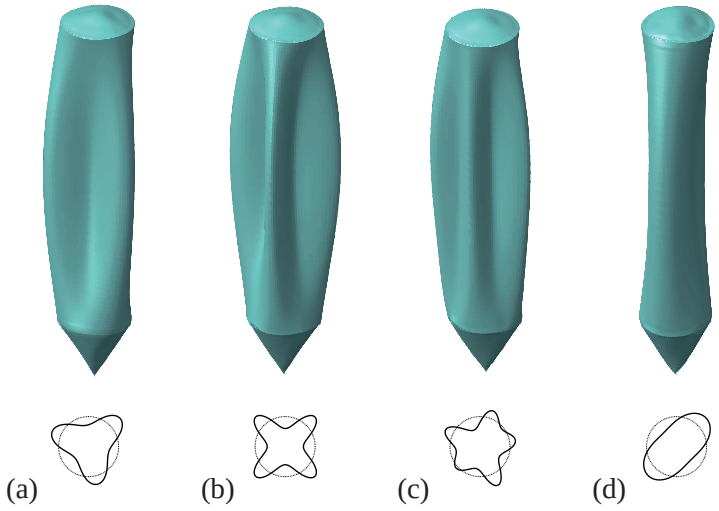

Figure 2: Selection of ovalling eigenmodes of a single silo: (a) mode $\mathbf{\Phi}_1 = (1, 3)$ at 3.96 Hz, (b) mode $\mathbf{\Phi}_4 = (1, 4)$ at 4.11 Hz, (c) mode $\mathbf{\Phi}_5 = (1, 5)$ at 5.34 Hz and (d) mode $\mathbf{\Phi}_{11} = (1, 2)$ at 7.83 Hz.

As mentioned, a FE approach is used to discretize the governing structural equations in the Abaqus software package 6.10 (2010). To accommodate an easy transfer of the aerodynamic pressures on the silo walls to the mesh of the structural model in the coupled simulations (section 4), the mesh of the FE model was chosen conforming to the mesh on the silo walls in the 3D CFD simulations. Because the cone at the bottom of the silo structure is covered by the building below the silo, no CFD grid is defined for this part of the structure and a separate mesh is made compatible with that of the superstructure. Shell elements with linear FE interpolation functions are used for all silo elements and the following material properties for aluminium are used: density ρ = 2700 kg/m^3, Young's modulus E = 67.6 GPa and Poisson's ratio ν = 0.35. The silo structures are bolted to a steel framework in the supporting building at 4 discrete points.

A list of the mass normalized eigenmodes $\mathbf{\Phi}$ of the structure corresponding to the lowest natural frequencies f_{eig} is given in table 1. Note that most of the mode shapes come in pairs: e.g. $\mathbf{\Phi}_1$ and $\mathbf{\Phi}_2$ are both classified as mode shapes $(1, 3)$ but are mutually orthogonal.

The visually detected pattern of vibrations at the lee side of the silo group during the 2002 storm is believed to have been ovalling mode shapes $(1, 3)$ and $(1, 4)$, with the lowest natural frequencies of the silo structure. Measurements during normal wind loading have also shown that eigenmodes with 3 or 4 circumferential wavelengths have the highest contribution to the response of the silos (Dooms *et al.*, 2006).

$\boldsymbol{\Phi}_j$	(m,n)	$f_{\mathrm{eig},j}$ [Hz]	$\boldsymbol{\Phi}_j$	(m,n)	$f_{\mathrm{eig},j}$ [Hz]	$\boldsymbol{\Phi}_j$	(m,n)	$f_{\mathrm{eig},j}$ [Hz]
$\boldsymbol{\Phi}_1$	$(1,3)$	3.96	$\boldsymbol{\Phi}_7$	$(1,5)$	5.70	$\boldsymbol{\Phi}_{13}$	$(2,5)$	8.19
$\boldsymbol{\Phi}_2$	$(1,3)$	3.97	$\boldsymbol{\Phi}_8$	$(1,5)$	5.71	$\boldsymbol{\Phi}_{14}$	$(2,6)^*$	8.62
$\boldsymbol{\Phi}_3$	$(1,4)$	3.99	$\boldsymbol{\Phi}_9$	$(1,6)$	7.72	$\boldsymbol{\Phi}_{15}$	$(2,4)$	8.85
$\boldsymbol{\Phi}_4$	$(1,4)$	4.11	$\boldsymbol{\Phi}_{10}$	$(1,6)$	7.72	$\boldsymbol{\Phi}_{16}$	$(2,4)$	9.10
$\boldsymbol{\Phi}_5$	$(1,5)$	5.34	$\boldsymbol{\Phi}_{11}$	$(1,2)$	7.83	$\boldsymbol{\Phi}_{17}$	$(2,6)$	9.62
$\boldsymbol{\Phi}_6$	$(1,5)$	5.35	$\boldsymbol{\Phi}_{12}$	$(2,5)$	8.18	$\boldsymbol{\Phi}_{18}$	$(2,6)$	9.72

Table 1: Structural natural frequencies f_{eig} of the lowest ovalling mode shapes of the silo structure. Every mode shape $\boldsymbol{\Phi}_j$ is determined by a couple (m,n) while for $\boldsymbol{\Phi}_{14}$ the notation $(2,6)^*$ is used to characterize its hybrid mode shape combining $(2,6)$ and $(1,2)$.

4 Wind-structure interaction

To investigate the onset of the wind-induced ovalling vibrations the coupled wind-structure interaction problem has to be considered as a whole. For this reason, both one-way and two-way coupling simulations are performed, as mentioned in the introduction. It is very valuable to assess the necessity of the computationally much more intensive two-way coupling simulations.

A partitioned approach is followed in all simulations implying that both the structural and flow solver are maintained as separated solvers (e.g. two black-box solvers) and the interaction between both domains is incorporated only at the interface. This approach allows to use the numerical models in the previous sections without alterations. In this framework, the structural FE solver (section 3) can be denoted as follows:

$$\mathcal{S}\left[\mathbf{P}(t)\right] = \mathbf{U}(t) \tag{1}$$

where $\mathbf{U}(t)$ are the displacements of the structure and $\mathbf{P}(t)$ are the aerodynamic pressures acting on the structure. Similary, the numerical CFD solver for the wind flow (section 2) can be expressed as:

$$\mathcal{F}\left[\mathbf{U}(t)\right] = \mathbf{P}(t) \tag{2}$$

4.1 One-way coupling

In the one-way coupling simulations, the 3D aerodynamic surface pressures on the silo walls are determined first in the CFD simulations (equation 2) with the structural displacements assumed to be zero in these simulations: $\mathcal{F}\left[\mathbf{0}\right] = \mathbf{P}(t)$. Afterwards, the wind pressures are imposed as a transient external load on the 3D FE model of the silo and the dynamic structural response of the silo $\mathbf{U}(t)$ can be calculated with equation 1. An unconditionally stable direct time integration scheme is used in the structural solver.

The response of a silo to the wind pressures is shown at three snapshots in time in figure 3. The deformation of the silo structure is clearly dominated by a static deformation but small amplitude vibrations are present as well. To determine which mode shapes are contributing to the structural response, it is interesting to calculate the modal deformation energy of the structural response using modal projection techniques.

The deformation energy $E_{\mathrm{d}}(t)$ can be easily calculated from the known structural displacements $\mathbf{U}(t)$ and with the knowledge of the stiffness matrix $\mathbf{K}$ used in the FE model of the structure:

$$E_{\mathrm{d}}(t) = \frac{1}{2}\,\mathbf{U}^{\mathrm{T}}(t)\,\mathbf{K}\,\mathbf{U}(t) \tag{3}$$

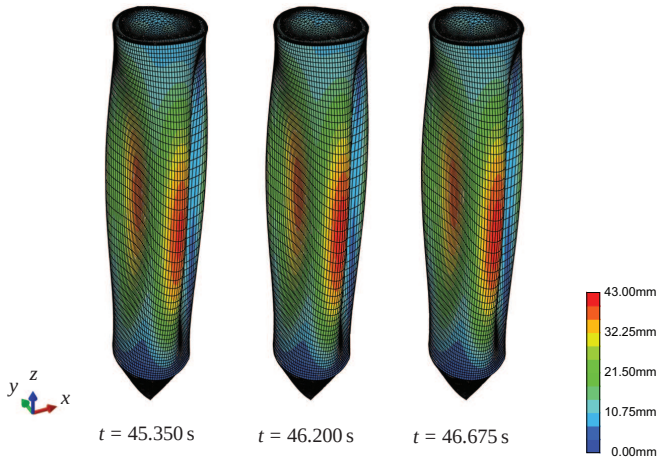

Figure 3: Deformation of the silo structure subjected to transient 3D wind pressures at $t = 45.350\,\mathrm{s}$, $t = 46.200\,\mathrm{s}$ and $t = 46.675\,\mathrm{s}$.

By applying modal decomposition of the structural deformations $\mathbf{U}(t) = \boldsymbol{\Phi}\boldsymbol{\alpha}(t)$ where $\boldsymbol{\alpha}(t)$ represent the modal coordinates, the energy content of each structural mode shape in the response can be quantified:

$$\begin{aligned} E_{\mathrm{d}}(t) &= \frac{1}{2}\,\boldsymbol{\alpha}^{\mathrm{T}}(t)\,\boldsymbol{\Phi}^{\mathrm{T}}\,\mathbf{K}\,\boldsymbol{\Phi}\,\boldsymbol{\alpha}(t) = \frac{1}{2}\,\boldsymbol{\alpha}^{\mathrm{T}}(t)\,\mathrm{diag}\{\omega_j\}^2\,\boldsymbol{\alpha}(t) \\ &= \frac{1}{2}\sum_{j=1}^{N}\omega_j^2\alpha_j^2(t) = \sum_{j=1}^{N}E_{\mathrm{d},j}(t) \end{aligned} \tag{4}$$

Only the lowest eigenmodes are expected to be relevant for the dynamic response of the structure to a typical low frequency wind excitation. It is therefore unwise to consider the entire orthonormal base of mode shapes. Instead, a subset of mode shapes $\boldsymbol{\Phi}_{\mathrm{s}}$ with the lowest eigenfrequencies is used and it can be shown that the above expressions hold if an alternative modal projection is used with this limited subset of mode shapes: $\boldsymbol{\alpha}(t) = \boldsymbol{\Phi}_{\mathrm{s}}^{\mathrm{T}}\mathbf{M}\mathbf{U}(t)$.

Figure 4 shows the modal deformation energy $E_{\mathrm{d},j}(t)$ for the first 20 mode shapes. It is clear that only some of these mode shapes have a significant contribution to the structural response of the silo. Before considering the different excited mode shapes however, a clear distinction should be made beween static and fluctuating components in the response. On the one hand, it is clear that the mean, time averaged component of the modal deformation is related to the extent that a mode shape is excited in the static deformation. In the fluctuating parts on the other hand, a further distinction has to be made between two fluctuating components. The first is related to the large scale turbulent eddies present in the incident wind flow attacking the structure, resulting in bands of low-frequency vibrations in the structural response. Because of this, these vibrations could also be categorized as 'quasi-static' sway of the structure, since no resonant effects are at play. The second component contains the higher frequency fluctuations, corresponding to the eigenfrequency of the considered mode shape and therefore related to forced resonance.

In this light, it is clear that mainly mode shapes $\boldsymbol{\Phi}_2 = (1,3)$, $\boldsymbol{\Phi}_4 = (1,4)$ and $\boldsymbol{\Phi}_6 = (1,5)$ have a significant contribution in the higher frequency dynamic response of the silo structure. The deformation energy of all these excited mode shapes is oscillating at a frequency coinciding with their natural frequencies. Superimposed, there are also low-frequency fluctuations, mainly in mode shapes $\boldsymbol{\Phi}_2$ and

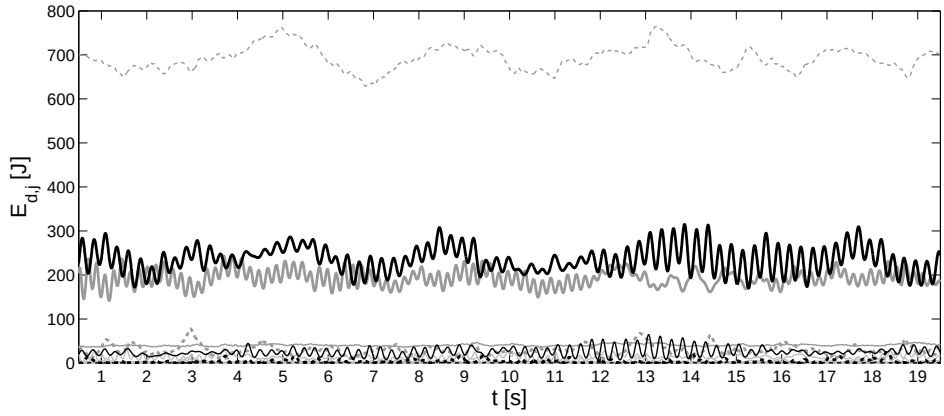

Figure 4: Modal deformation energy $E_{\mathrm{d},j}(t)$ for the first 20 mode shapes, based on the structural response in the coarse grid one-way coupling simulation of a single silo: $\mathbf{\Phi}_1 = (1,3)$ (dashed bold black line), $\mathbf{\Phi}_2 = (1,3)$ (solid bold black line), $\mathbf{\Phi}_3 = (1,4)$ (dashed thin black line), $\mathbf{\Phi}_4 = (1,4)$ (solid thin black line), $\mathbf{\Phi}_5 = (1,5)$ (dashed bold grey line), $\mathbf{\Phi}_6 = (1,5)$ (solid bold grey line), $\mathbf{\Phi}_{14} = (2,6)^*$ (dashed thin grey line), $\mathbf{\Phi}_{18} = (2,6)$ (solid thin grey line), and the remaining mode shapes $\mathbf{\Phi}_j$ (solid thin light grey lines, with small energy content).

$\mathbf{\Phi}_6$. Furthermore, the latter are also explicitly excited statically as can be observed in figure 3. By considering the pressure distribution on the silo surface, it is also explained why typically only one of each pair of orthogonal mode shapes is excited. Depending on the orientation of the mode shape with respect to the wind direction, e.g. from the two mode shapes $(1,3)$, where mode shape $\mathbf{\Phi}_2$ is excited while $\mathbf{\Phi}_1$ is not. Somewhat unexpected when the pressure distribution on the silo surface is considered is the contribution of mode shapes $\mathbf{\Phi}_{14} = (2,6)^*$ and, although less pronounced, mode shape $\mathbf{\Phi}_{18} = (2,6)$ to the deformation energy. The notation $(2,6)^*$ is used to characterize the hybrid mode shape combining $(2,6)$ and $(1,2)$. The excitation of these mode shapes is however directly related to the location of the connections of the silo to the environment. Both mode shapes $\mathbf{\Phi}_{14}$ and $\mathbf{\Phi}_{18}$ have a mainly 'quasi-static' component and are only little excited dynamically.

4.2 Two-way coupling

For the two-way coupling, the fluid and structural solvers are interacting in every time step so that the structural deformation is influenced by the wind pressures in every time step and vice versa. To ensure equilibrium at the wind-structure interface in every time step, several Gauss-Seidel coupling iterations between the solvers are performed. For the present simulations, five iterations per time step are needed to reach convergence. Because of these coupling iterations between the solvers, the computational effort for the two-way coupling simulations is much larger than in the one-way coupling approach. It is therefore interesting to assess the necessity of performing these computationally much more imposing simulations.

Other computational issues as a result of the two-way coupling include possible interpolation issues at the interface for the transfer of displacements and pressures on the one hand and the solution of the wind flow simulations on a deforming domain on the other hand. The first issue is bypassed by using identical meshes at the interface in both the structural and the flow solver. For the second, the mesh movement of the computational grid in the flow solver is made possible using the arbitrarian Lagrangian-Eulerian (ALE) description as implemented in Ansys Fluent 14.0 (2011).

Similarly as for the one-way coupling approach, the dynamic structural response is calculated and

the modal deformation energy is determined. The results for the two-way coupling simulations are shown in figure 4. Although the modal deformation energy determined for the one-way (figure 5) and for the two-way simulations (figure 5) are not identical, qualitatively the results correspond very well. The same mode shapes are found to contribute to the structural response with similar amplitudes. Furthermore, it has to be noted that due to the 'random' character of the transient incoming turbulent wind flow, the two signals are not expected to be identical. These results were found in two separate simulations and should therefore only be compared in terms of statistical agreement.

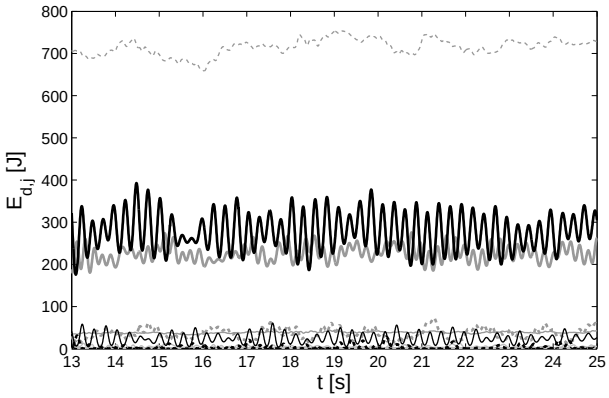

Figure 5: Modal deformation energy $E_{\mathrm{d},j}(t)$ for the first 20 mode shapes, based on the structural response in the coarse grid two-way coupling simulation of a single silo: $\mathbf{\Phi}_1 = (1,3)$ (dashed bold black line), $\mathbf{\Phi}_2 = (1,3)$ (solid bold black line), $\mathbf{\Phi}_3 = (1,4)$ (dashed thin black line), $\mathbf{\Phi}_4 = (1,4)$ (solid thin black line), $\mathbf{\Phi}_5 = (1,5)$ (dashed bold grey line), $\mathbf{\Phi}_6 = (1,5)$ (solid bold grey line), $\mathbf{\Phi}_{14} = (2,6)^*$ (dashed thin grey line), $\mathbf{\Phi}_{18} = (2,6)$ (solid thin grey line), and the remaining mode shapes $\mathbf{\Phi}_j$ (solid thin light grey lines, with small energy content).

The vibration amplitudes in the two-way coupling simulations are in the same order of magnitude as in the one-way coupling simulations (maximum total displacements of about 4 to 5 cm). Although smaller than the the observed vibration levels (order of magnitude 10 cm dynamic displacement), it is possible that vibrations computed here for a single isolated silo will be larger in the group arrangement (Hillewaere *et al.*, 2012).

5 Conclusions

In order to clarify the observed ovalling vibrations in a group of 8 by 5 silos during a storm, 3D wind-structure interaction simulations are performed. First a better understanding of the wind flow around a single silo is investigated by performing 3D DDES simulations of the turbulent wind flow around the single silo structure. Afterwards a FE model is set up for the silo structure to numerically determine the ovalling mode shapes and to be used in the coupled wind-structure interaction problem.

Both one-way and two-way coupling simulations are performed. In the one-way coupling simulations the aerodynamic pressures are applied as a transient external load on the FE model of the silo, without feedback of the structural deformation to the wind flow domain. In the two-way coupling simulations, this feedback is given in each time step and coupling iterations have to be performed to ensure equilibrium on the wind-structure interface. Both approaches yield very similar results: the same mode shapes with low natural frequencies are excited in both models and structural displacements are similar as well. Although the observed vibration levels are still small when compared to the vibrations observed during the 2002 storm, they coincide with the observed vibration patterns in the

group. For the single silo configuration, the more cumbersome and time-consuming two-way coupling simulations do not yield a better prediction of the ovalling vibrations. However, it is possible that this two-way coupling may be more important for the closely spaced group of silos.

References

FLUENT 14.0, 2011. *User's Guide*. Ansys Inc.

Abaqus 6.10, 2010. *User's Manual*. Dassault Systèmes Simulia Corp.

Dooms, D., Degrande, G., De Roeck, G., & Reynders, E. 2006. Finite element modelling of a silo based on experimental modal analysis. *Engineering Structures*, **28**(4), 532–542.

Hillewaere, J., Dooms, D., Van Quekelberghe, B., Degroote, J., Vierendeels, J., De Roeck, G., Lombaert, G., & Degrande, G. 2012. Unsteady Reynolds averaged Navier-Stokes simulation of the post-critical flow around a closely spaced group of silos. *Journal of Fluids and Structures*, **30**, 51–72.

Kraichnan, R. 1970. Diffusion by a Random Velocity Field. *Physics of Fluids*, **11**, 21–31.

Menter, F.R., & Kuntz, M. 2002. Adaptation of eddy-viscosity turbulence models to unsteady separated flow behind vehicles. *In:* McCallen, R., Browand, R., & Ross, J. (eds), *Symposium on the aerodynamics of heavey trucks, buses and trains*. Monterey, USA: Springer, Berlin Heidelberg New York, 2004.

Païdoussis, M.P., Price, S.J., & Suen, H.C. 1982. Ovalling Oscillations of Cantilevered and Clamped-Clamped Cylindrical Shells in Cross Flow: An Experimental Study. *Journal of Sound and Vibration*, **83**(4), 533–553.

Smirnov, A., Shi, S., & Celik, I. 2001. Random Flow Generation Technique for Large Eddy Simulations and Particle-Dynamics Modeling. *Journal of Fluids Engineering, Transactions of the ASME*, **123**, 359–371.

Spalart, P.R., Jou, W.-H., Strelets, M., & Allmaras, S.R. 1997. Comments on the feasibility of LES for wings, and on a hybrid RANS/LES approach. *In: Proceedings of first AFOSR international conference on DNS/LES*. Ruston, Louisiana: Greyden Press.

Tominaga, Y., Mochida, A., Yoshie, R., Kataoka, H., Nozu, T., Yoshikawa, M, & Shirisawa, T. 2008. AIJ guidelines for practical applications of CFD to pedestrian wind environment around buildings. *Journal of Wind Engineering and Industrial Aerodynamics*, **96**, 1749–1761.